Review Article

Optical coherence tomography: A guide to interpretation of common macular diseases

Muna Bhende[1], Sharan Shetty[1], Mohana Kuppuswamy Parthasarathy[1,2], S Ramya[1]

Optical coherence tomography is a quick, non invasive and reproducible imaging tool for macular lesions and has become an essential part of retina practice. This review address the common protocols for imaging the macula, basics of image interpretation, features of common macular disorders with clues to differentiate mimickers and an introduction to choroidal imaging . It includes case examples and also a practical algorithm for interpretation.

Key words: Macular diseases, optical coherence tomography biomarkers, optical coherence tomography

Access this article online

Website: www.ijo.in

DOI: 10.4103/ijo.IJO_902_17

Quick Response Code:

Optical coherence tomography (OCT) is an optical analog of ultrasound imaging that uses low coherence interferometry to produce cross-sectional images of the retina. It captures optical scattering from the tissue to decode spatial details of tissue microstructures. It uses infrared light from a super-luminescent diode that is divided into two parts: one of which is reflected from a reference mirror and the other is scattered from the biological tissue. The two reflected beams of light are made to produce interference patterns to obtain the echo time delay and their amplitude information that makes up an A-Scan. A-Scans that are captured at adjacent retinal locations by transverse scanning mechanism are combined to produce a 2-dimensional image.[1] The stages of evolution of various types of OCT from the original time-domain OCT to spectral domain (SD-OCT) and swept-source OCT (SSOCT) are shown in Fig. 1 and the corresponding images are shown in Fig. 2. Table 1 is a brief comparison of the salient features of the three types of OCT.

Optical Coherence Tomography Scan Protocols

Scan protocols used in the more widely used SD-OCT systems are mentioned in this section. The commonly used scan protocols for macular scanning are three-dimensional (3D) scan, radial scan, and raster scan [Fig. 3]. A 3D scan consists of a number of horizontal line scans [Fig. 4, left] composing a 6 mm × 6 mm or 7 mm × 7 mm or 12 mm × 9 mm rectangular box. It generates a 3D view of the image which enables the implementation of advanced, complex analysis, for example, C-scan, topographic maps, and cyst volume and gives a holistic view of the macula. Raster scan is a series of parallel line scans that can be oriented in any angle and is of higher resolution [Fig. 4, right]. The radial scan consists of 6–12 line scans arranged in equal angles with common axis [Fig. 5]. When the axis coincides with the fovea, the relationship of the lesion to the fovea is documented. These scan protocols may differ in length, density, or resolution depending on the OCT system used [Fig. 6].

Optical Coherence Tomography Scan Acquisition Procedure

A minimum pupil diameter of 3 mm is required to obtain a good OCT image. An appropriate scanning protocol is selected to scan the retinal area of interest and a live OCT window is seen. The patient is instructed to look at the internal target at the center (for macular scanning) or an external target where appropriate. Once the fundus image on the monitor is focused, the OCT image appears on the monitor, focus is enabled by correcting refractive errors. Make sure that the OCT image is upright and straight and the reference scan pattern is centered on the fovea or the area of interest. Adjust the light entry point across the pupil to get the best signal strength. Repeat the procedure with other scan protocols if necessary. The saved

[1]Shri Bhagwan Mahavir Vitreoretinal Services, Medical Research Foundation, Chennai, Tamil Nadu, India, [2]School of Optometry and Vision Science, University of Waterloo, Waterloo, ON N2L 3G1, Canada

Correspondence to: Dr. Muna Bhende, Shri Bhagwan Mahavir Vitreoretinal Services, Medical Research Foundation, 18 College Road, Chennai - 600 006, Tamil Nadu, India. E-mail: drmuna@snmail.org

Manuscript received: 23.09.17; Revision accepted: 16.11.17

Cite this article as: Bhende M, Shetty S, Parthasarathy MK, Ramya S. Optical coherence tomography: A guide to interpretation of common macular diseases. Indian J Ophthalmol 2018;66:20-35.

Table 1: Comparison of salient features of the three types of optical coherence tomography

Type of OCT	Image acquisition	Scanning speed	Axial resolution	Transverse resolution	Range of imaging
Time domain	Superluminescent diode (810 nm) single photon detector, moving mirror	400 A-scans per second	10 μm	20 μm	Vitreoretinal interface to RPE
Spectral domain	Broadband superluminescent diode source (840 nm), array of detectors, fixed mirror	27,000-70,000 A-scans per second	5-7 μm	14-20 μm	Posterior cortical vitreous to sclera using EDI mode
Swept source	Swept-source tunable laser (1050 nm), single detector	100,000-400,000 A-scans per second	5 μm	20 μm	Posterior cortical vitreous to sclera (superior to SD OCT with EDI)

RPE: Retinal pigment epithelium, EDI: Enhanced-depth imaging, SD OCT: Spectral-domain OCT, OCT: Optical coherence tomography

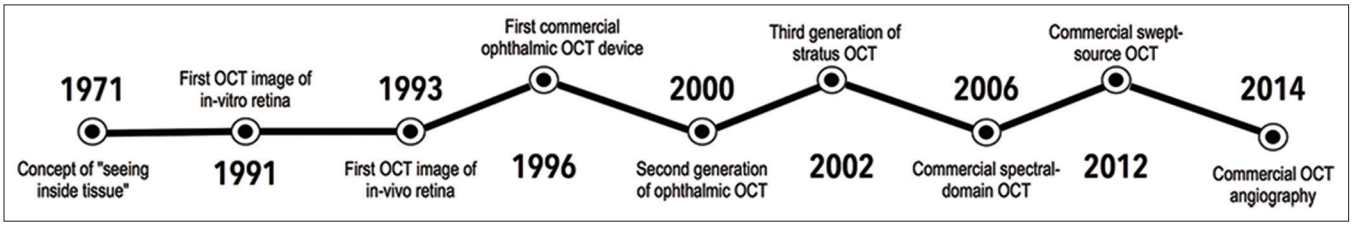

Figure 1: Time line showing the evolution of various types of optical coherence tomography

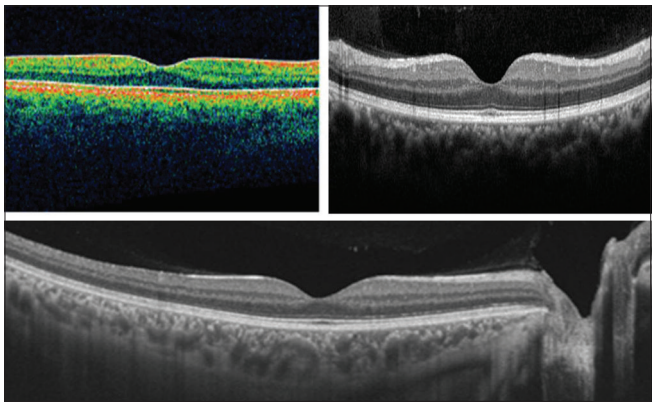

Figure 2: Images of time domain optical coherence tomography (top left), spectral domain optical coherence tomography (top right), and swept-source optical coherence tomography (bottom) of normal macula

OCT scans are analyzed both qualitatively and quantitatively. The OCT view window consists of the analyzed OCT images with its corresponding fundus image showing the orientation of the OCT scan. The analysis report varies with different OCT systems. In general, all machines have a thickness map displaying the average retinal thickness values in 1 mm, 3 mm, and 6 mm diameter circles divided into sectors with color map. Warm colors indicate thicker retinal areas and cool colors indicate thinner retinal areas [Fig. 7].

Measurements

Retinal thickness is a reproducible and common quantitative measurement that is used to monitor the disease process or treatment response using OCT.[2] Every OCT system has an inbuilt segmentation algorithm that identifies the differences in reflectance of the retinal layers and borders and then places lines over the inner and outer border of the retina. The total retinal thickness is the measurement of the distance between these two segmentation lines. Some OCT machines can delineate individual layers of the retina including the outer segments of the photoreceptors and retinal pigment epithelium (RPE). Manual correction of segmentation lines is possible in case of segmentation artifacts and retinal thickness can be measured manually using the inbuilt caliper function. The scan protocols, namely, 3D cube scan and radial scan generates the early treatment diabetic retinopathy study grid with the thickness values displayed in each sector. Central subfield thickness corresponding to the central 1 mm average retinal thickness has high diagnostic value and it correlates with visual acuity.[3] Retinal thickness change between two visits with color coding helps in identifying the absolute change in the areas of thickening/thinning. Comparison of retinal thickness measurements between OCT machines has to be done with caution because of the differences in the placement of segmentation lines that define the retinal thickness. All OCT instruments take the internal limiting membrane as the inner retinal border. The outer retinal border could be any one of the three hyper-reflective outer retinal layers, for example, Spectralis and Cirrus high-definition OCT take the outer most layer, RPE while RTVue takes the inner border of the second hyper-reflective line, the interdigitation zone.[4] Therefore, the normative value for retinal thickness is unique to the machine used and the ethnic background of the subject.[5]

Table 2 describes the common terminologies used while measuring the thickness and change of thickness in the macular region.[6]

Artifacts on Optical Coherence Tomography

OCT artifacts could be patient related, operator-related, and software related. While patient- and operator-related artifacts can be controlled to some extent, software-related errors are inevitable and most common. Patient-related artifacts are mostly due to eye movements, which can be controlled by eye

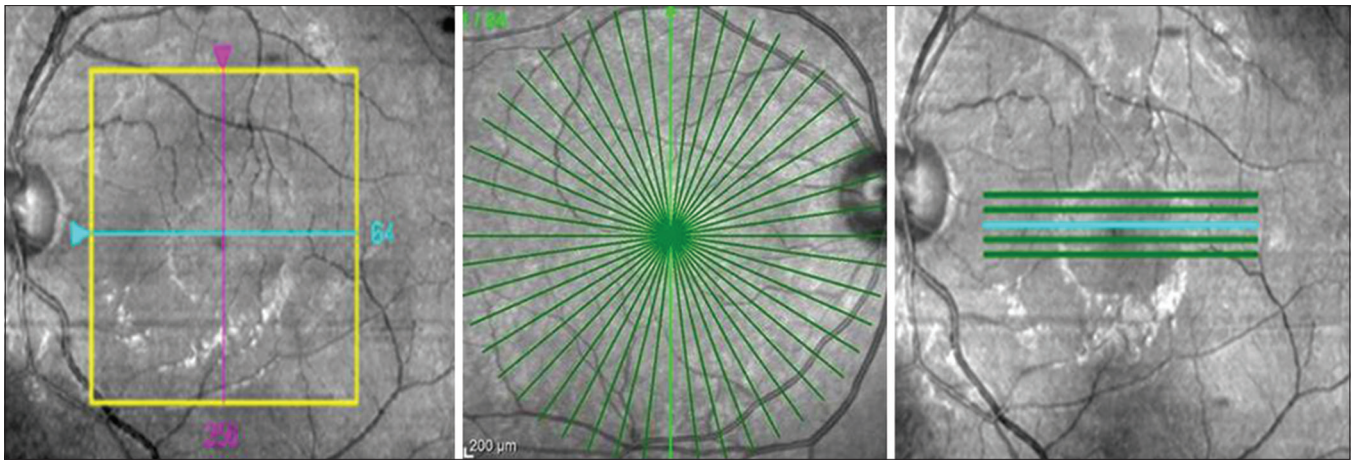

Figure 3: Commonly used protocols for spectral domain optical coherence tomography: Macular cube (left), radial line scan (center), and raster scan (right)

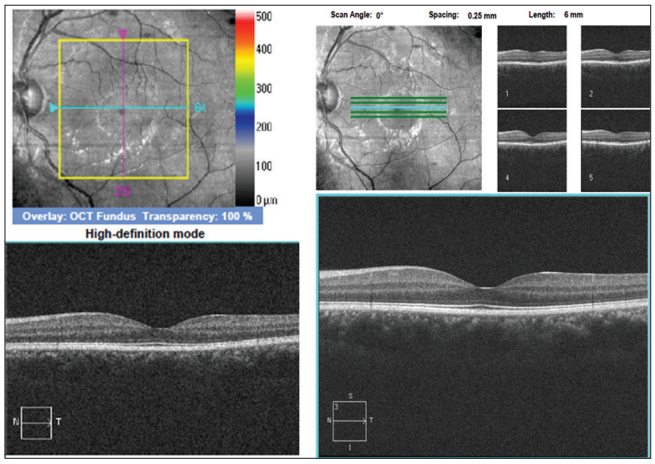

Figure 4: Macular cube 512 × 128 scan (left) High definition 5-line raster scan (right) Images from Cirrus OCT, Zeiss

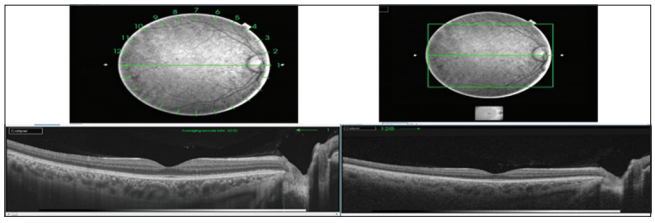

Figure 6: 12 mm radial scan comprising 12-line scans (LEFT) Three-dimensional macula cube scan of 12 mm × 9 mm dimension (RIGHT) Images from Atlantis DRI OCT, Topcon

tracking software. Operator-related artifacts include decentered scans, out of registration due to cut images and degraded images due to poor focus. Software-related artifacts are mostly due to failed segmentation algorithms resulting in misidentification of inner, outer retinal boundaries, and incomplete segmentation artifacts.[7] Certain artifacts are associated with a particular disease, for instance, segmentation failure occurs commonly in diseases such as age-related macular degeneration (AMD), vitreomacular traction.[8] Artifacts in the center 1 mm area of scans are infrequent but when present, can affect the center subfield thickness measurements.[9]

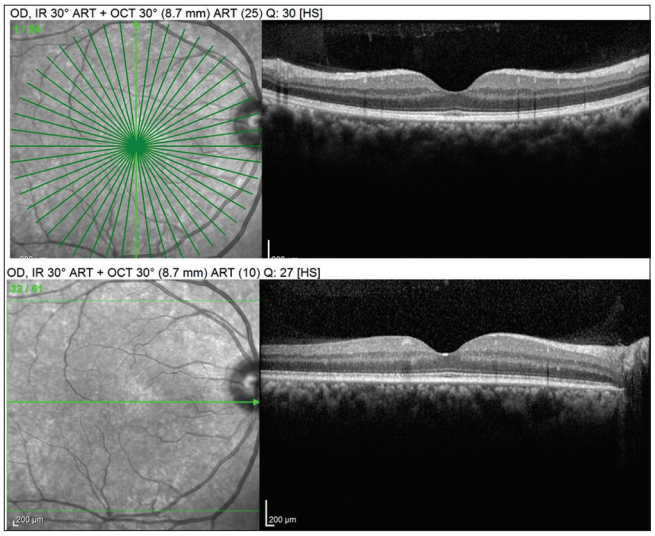

Figure 5: Radial scan 24 lines of 30° (8.7 mm) scan with ART 25 taken in high-speed mode (TOP) Three-dimensional volume scan of posterior pole of 61 horizontal line scans with ART 10 (BOTTOM). Images from Spectralis OCT, Heidelberg

Optical Coherence Tomography Features in Common Macular Disorders

Being noninvasive, quick and reproducible, OCT is used commonly in the diagnosis, and the management of optic nerve and retinal disorders not only for diagnosis but also as a follow-up tool both in clinical practice and in many multicentric trials. Standardized protocols for measurements as well as classic appearances attributable to different structural changes have converted an OCT image into an optical biopsy. The following sections aim to serve as a guide to the OCT features of common retinal conditions along with their relevance in terms of prognosis and also distinguishing features between often misdiagnosed situations.

An international panel with expertise in retinal imaging (International Nomenclature for OCT Panel) has provided a lexicon for the classification of anatomical

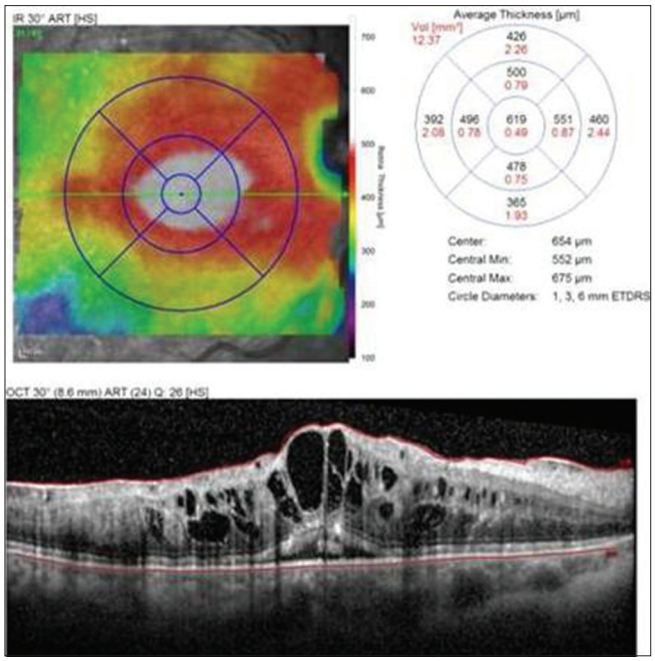

Figure 7: Retinal thickness map: Top left image shows the color-coded macular thickness map showing thickening at the macular region and macular thickness values are seen in 1 mm, 3 mm, and 6 mm circles in the top right image. Bottom image shows the corresponding spectral domain optical coherence tomography image

landmarks of identifiable on SD-OCT in the normal macula.[10] As a general guide, based on relative reflectivity, the retinal and choroidal layers are divided into zones (areas which have specific reflective structures but cannot be easily distinguished by clear-cut margins and lack proven histologic evidence for the same) and bands or layers (areas which are discrete and well defined and have a proven histologic correlation). A listing of the zones and their reflectivity are seen in Table 3. Table 4 lists out the reflectivity of common pathological changes seen on OCT.

Optical Coherence Tomography in Disorders of the Vitreomacular Interface

These include vitreomacular adhesion (VMA), vitreomacular traction (VMT), and macular hole.

The International Vitreomacular Traction Study Group classification is OCT-based and designed to be used as a therapeutic or research guide as well as a possible predictor of treatment outcomes.[11]

Perifoveal posterior vitreous detachment with a posterior cortical vitreous attachment within 3 mm of the fovea is considered as VMA if there are no secondary changes in the contour or within the retina. If the area of attachments is ≤1500 µm, it is considered focal and if >1500 µm it is considered broad.[12]

All of the following anatomic criteria must appear on at least 1 B-mode OCT scan to classify an eye as having VMT: (1) evidence of perifoveal vitreous cortex detachment from the retinal surface; (2) macular attachment of the vitreous cortex within a 3-mm radius of the fovea; and (3) association

Table 2: Definitions of commonly used landmarks and measurements on optical coherence tomography

Retinal thickness	Value in microns of the distance between the OCT layers assumed to be the RPE and the internal limiting membrane
Retinal thickening	Calculated value equal to the thickness minus the population mean for the variable under consideration (either CPT or CSMT)
CP	The intersection of the 6 radial scans of the fast macular thickness protocol of the OCT
CPT	Average of the thickness values for the 6 radial scans at their point of intersection
CS	Circular area of diameter 1 mm centered around the CP; 128 thickness measurements are made in this circular area in the fast macula protocol
CSMT	Mean value of the 128 thickness values obtained in the CS
Absolute change in thickness	Difference in the thickness between 2 measurements made at different times
Relative change in thickness	Absolute change in thickness divided by the baseline thickness
Relative change in thickening	Absolute change in thickness (or thickening) divided by the baseline thickening

CP: Center point, CPT: CP thickness, CS: Central subfield, CSMT: CS mean thickness, OCT: Optical coherence tomography, RPE: Retinal pigment epithelium

Table 3: Anatomical layers as seen on optical coherence tomography and their reflectivity

Hyperreflective bands	Posterior cortical vitreous, NFL, IPL, OPL, ELM, and RPE/Bruch's membrane complex
Hyperreflective zones	Ellipsoid zone, interdigitation zone
Hyporeflective bands	GCL, INL, Henle's NFL and ONL, outer segments of photoreceptors
Hyporeflective zones	Myoid zone The choriocapillaris, inner and outer choroidal layers occupy a zone of hyporeflective spaces with hyperreflective outlines of various sizes. The boundaries are ill-defined
Choroidoscleral junction	Zone of variable reflectivity at the outer border of the choroidal vascular profiles

NFL: Nerve fiber layer, IPL: Inner plexiform layer, OPL: Outer plexiformlayer, ELM: External limiting membrane, RPE: Retinal pigment epithelium, GCL: Ganglion cell layer, INL: Inner nuclear layer, ONL: Outer nuclear layer

Table 4: Common causes of abnormal reflectivity on optical coherence tomography

Reduced reflectivity	Fluid (retinal edema, subretinal fluid, sub-RPE fluid)
Increased reflectivity	Hard exudates, calcification, hemorrhages, fibrosis Epiretinal and vitreous membranes, CNV, RPE, hyperplasia RPE atrophy causing hyperreflectivity of the choroid

RPE: Retinal pigment epithelium, CNV: Choroidal neovascularization

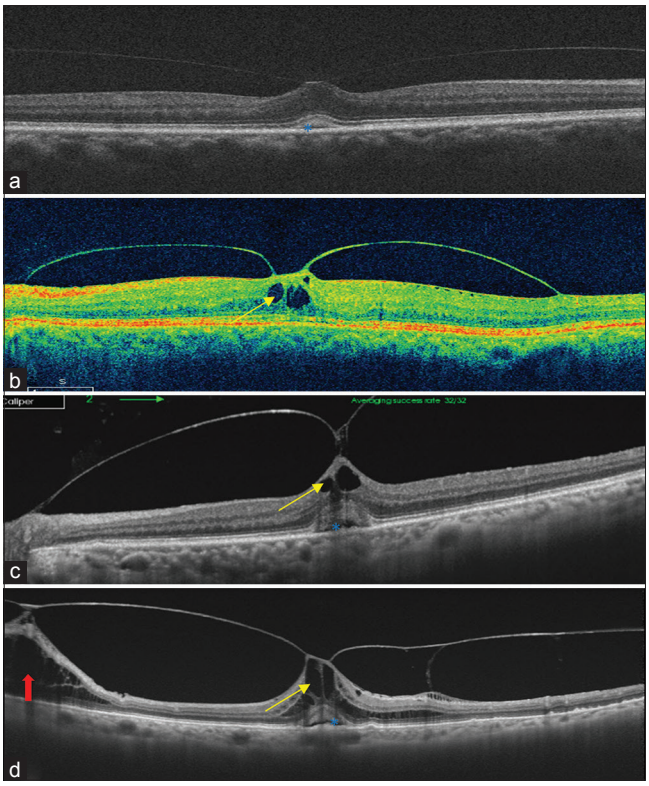

Figure 8: The figures show evidence of different stages of vitreomacular traction. (a) Spectral domain optical coherence tomography showing focal vitreomacular traction with a small subfoveal detachment (blue star). (b) Spectral domain optical coherence tomography showing focal vitreomacular traction with intraretinal cystic spaces (yellow arrow). (c) Swept-source optical coherence tomography showing focal vitreomacular traction with inner retinal cysts (yellow arrow) and a subfoveal detachment (blue star). (d) Swept-source optical coherence tomography showing vitreomacular traction with more extensive intraretinal cystic spaces (yellow arrow) and a subfoveal detachment (blue star). Vitreoschisis is also seen and a second area of traction away from the fovea red arrow)

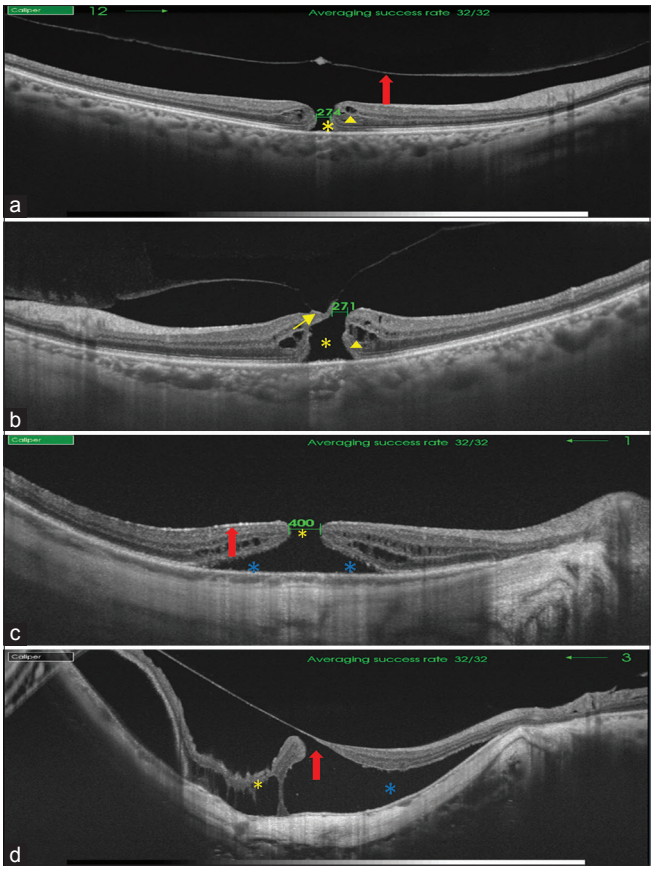

Figure 9: (a) Small macular hole (yellow star) with intraretinal cystoid spaces (yellow triangle). The posterior vitreous is detached with an operculum (red arrow). (b) Macular hole (yellow star) with posterior hyaloid attached to one edge (yellow arrow and intraretinal cystoid spaces (yellow triangle). (c) Macular hole (yellow star) with localized RD (blue star) and attached posterior hyaloid (red arrow). The sclera is seen clearly on swept-source optical coherence tomography in high myopia (d) Myopic eye showing macular schisis (yellow star), macular hole with posterior hyaloid attached to the edge (red arrow), and RD (blue star)

of attachment with distortion of the foveal surface, intraretinal structural changes, (pseudocysts, macular schisis, cystoid macular edema (CME), and subretinal fluid [SRF]), elevation of the fovea above the RPE, or a combination thereof, but no full-thickness interruption of all retinal layers.[11,13] Fig. 8 shows the various stages of VMT.

Both VMA and VMT are divided into isolated or concurrent based on the presence or absence of a preexisting retinal condition.

Full-thickness macular holes (FTMH) are defects in the fovea featuring absence of all neural retinal layers from the inner limiting membrane (ILM) to the RPE. These are classified based on their aperture size (minimum hole width) into small (≤250 μm), medium (>250–400 μm), or large (>400 μm) and also based on the presence or absence of VMT [Fig. 9] The concept of measuring the hole size is to predict outcomes after surgery which worsen as the hole size becomes larger.[14] A lamellar hole is a defect where the photoreceptors are intact at the base. This could present with an irregular foveal contour, a defect in the inner foveal layers without actual tissue loss or intraretinal splitting between the outer plexiform and outer nuclear layers (ONLs).[15] Macular pseudohole can be seen as invaginated or heaped foveal edges, Epiretinal membrane (ERM) with central opening, steep macular contour to the central fovea with near-normal central foveal thickness and no tissue loss.[16]

Optical Coherence Tomography in Choroidal Neovascular Membrane

Well-defined hyperreflective tissue between the RPE/Bruch's membranes (Type 1) or above the RPE (Type 2).[17,18] Type 3 choroidal neovascularization (CNV) features include sub-RPE CNV with intraretinal hyper reflective foci along with subretinal neovascularization and intraretinal cystoid changes.[19,20] The sequence of events in Type 3 is intraretinal followed by subretinal and finally sub-RPE proliferation. Fig. 10 shows the features of different types of CNV.

Type 1 neovascularization occurs primarily in AMD and similar entities with diffuse RPE/Bruch's membrane abnormalities such as cuticular drusen and malattia leventinese, as well as polypoidal choroidal vasculopathy (PCV). Type 2

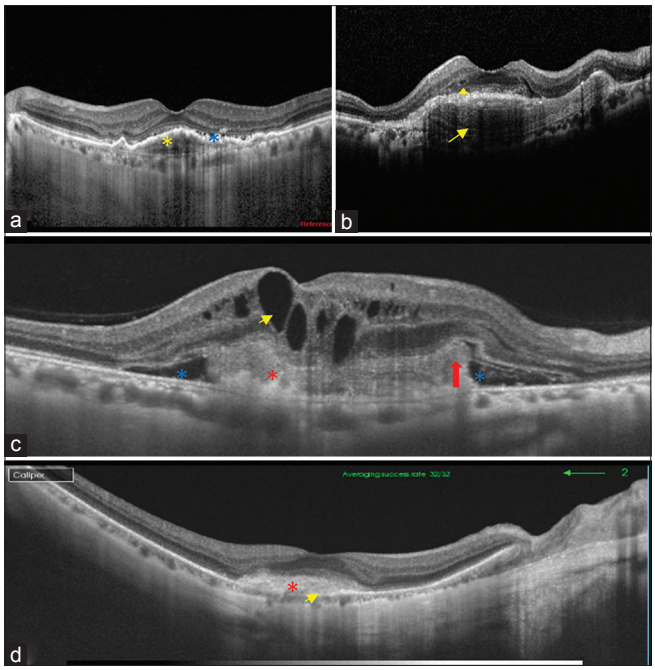

Figure 10: (a) Type 1 choroidal neovascularization with pigment epithelial detachment having heterogenous content (yellow star), trace subretinal fluid (blue star), and intraretinal hyperreflective dots. (b) Scarred fibrovascular pigment epithelial detachment with irregular surface, lamellar structure and shadowing (yellow arrow), overlying degenerative cystic spaces (yellow triangle). (c) Type 2 choroidal neovascularization showing a lesion of variable hyper reflectivity with a sharp edge that suggests the development of fibrosis (red arrow), subretinal fluid (blue star) intraretinal cystoid spaces (yellow arrow) and fibrosis (red star). (d) Swept-source optical coherence tomography in myopic choroidal neovascularization (red star) with breach in the retinal pigment epithelium (yellow arrow)

pattern is seen with more localized damage to the RPE/Bruch's membrane complex such as pathologic myopia with lacquer cracks, punctate inner choroidopathy, multifocal choroiditis and panuveitis, and choroidal rupture. It can also be seen in pattern and vitelliform macular dystrophies, ABCA4/Stargardt disease, reticular pseudodrusen, and pseudoxanthomaelasticum. Type 3 neovascularization is mostly seen in neovascular AMD, a similar angiogenic sequence may occur in eyes with macular telangiectasia Type 2 (idiopathic perifoveal telangiectasia).[21]

Associated features

Certain OCT-derived biomarkers have been identified that could predict the outcomes with treatment and most of these have been derived from AMD related studies.[22,23]

Central retinal thickness is not of as much importance in CNV management as in other conditions as the activity of the lesion has different manifestations in different retinal compartments which have a bearing on the ultimate visual outcome.[24,25] However, most clinical trials using OCT as a parameter continue to use retinal thickness change as a measure of outcome.[26,27]

Intraretinal cystoid fluid spaces are most often associated with Type 2 or 3 CNV where the lesion is above the RPE. In Type 1 or sub-RPE CNV, the intraretinal fluid appears late in the course of the disease.[21]

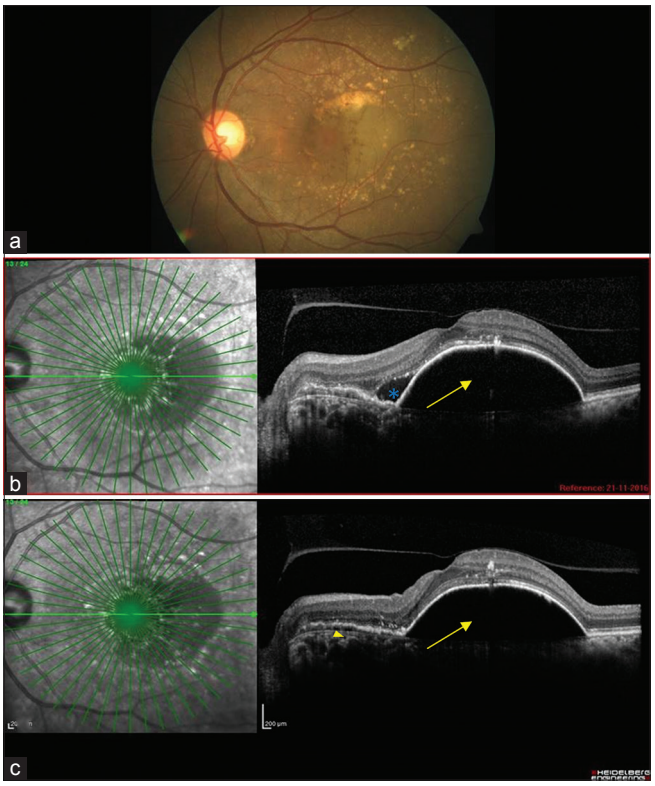

Figure 11: (a) Clinical photograph showing a pigment epithelial detachment with pigmentary changes on the surface, surrounded by drusen. (b) Spectral domain optical coherence tomography image showing a pigment epithelial detachment which is dome-shaped (yellow arrow) with an irregular surface at the border signifying both a serous and vascularized component. Subretinal fluid is also seen (blue star). (c) Spectral domain optical coherence tomography of the same eye, using eye tracking after multiple anti vascular endothelial growth factor injections. There is absence of subretinal fluid, reduction of the irregular component of the pigment epithelial detachment (yellow triangle), and persistence of the serous component (yellow arrow)

Exudative intraretinal fluid is seen as large circular or ovoid hyporeflective spaces overlying a pigment epithelial detachment (PED) or a Type 2/3 CNV. These respond well to antivascular endothelial growth factor (VEGF) therapy. However, the presence of intraretinal cystic spaces at baseline is associated with a poorer visual outcome.[28,29]

Degenerative intraretinal fluid is seen as small sharply demarcated hyporeflective spaces in the inner retina overlying areas of RPE atrophy or scarring.[30] These do not respond to anti-VEGF therapy. The intraretinal fluid that persists for more than 12 weeks of anti-VEGF monotherapy is considered degenerative fluid. Similar degenerative changes in the outer retina are referred to as outer retinal tubulations (ORTs) and are discussed subsequently.

SRF is an indicator of activity in all subtypes and is the first sign of activity in Type 1 CNV. The presence of SRF at the start of therapy has been shown to be a favorable sign for visual acuity improvement with therapy.[28,29]

Pigment epithelial detachment

There are various subtypes such as serous PED (with clear optically empty sub-RPE space), drusenoid (sub-RPE space is filled with moderately reflective material), fibrovascular (where

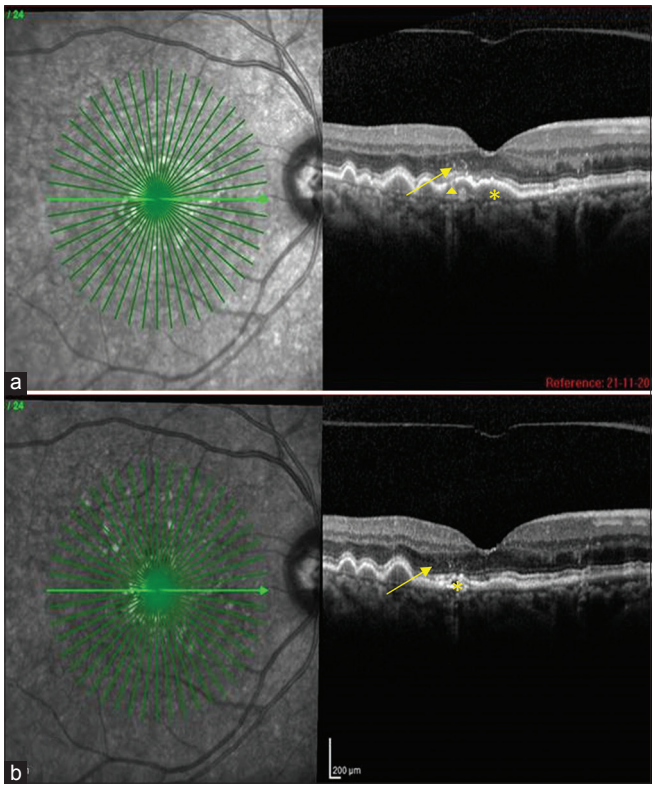

Figure 12: (a) Spectral domain optical coherence tomography image of an eye with multiple drusenoid deposits seen as smooth dome-shaped elevations of the retinal pigment epithelium with homogenous sub retinal pigment epithelium content (yellow star). The elevation closest to the fovea shows hyper reflective deposits both within the retinal pigment epithelium elevation and in the intraretinal space (yellow arrow) and an area of discontinuity of the retinal pigment epithelium (yellow triangle). (b) Follow-up optical coherence tomography 18 months later shows flattening of the lesion (yellow star) with reduction of the hyper reflective echoes (yellow arrow) signifying progression to atrophy

the sub-RPE space is filled with hyper reflective heterogeneous material) and hemorrhagic (where the surface appears highly reflective with shadowing due to the blood and the deeper layers are not seen) and mixed.[31] Fibrovascular PED is the hallmark of Type 1 CNV with changes in the overlying retina seen only in advanced cases. PED is also a feature of Type 3 CNV where both serous and fibrovascular PEDs are seen. Serous PEDs typically respond well to anti-VEGF therapy. In case of fibrovascular PED (FVPED), the height reduces but typically the neovascular tissue persists, giving rise to recurrences [Fig. 11]. Hence, monitoring of the height of the PED is as important as noting secondary intraretinal or subretinal changes during follow-up.

The subretinal hyperreflective material could represent a Type 2 or 3 CNV but can also contain subretinal hemorrhage, lipid, fibrous tissue, or exudate. The reflectivity of the CNV changes from moderate in the early stage to highly reflective as fibrosis develops.[32] The presence of such material under the fovea is a poor prognostic feature for visual acuity improvement.

Hyperreflective foci in the neurosensory retina form one of the newer, less understood OCT biomarkers in AMD.[32] Their origin is unclear, and they could represent migrating RPE cells, pigment-laden macrophages, microglial cells, or lipid. In early and intermediate AMD, the development of hyperreflective foci could signify conversion to a more advanced stage of atrophic or neovascular AMD[33] [Fig. 12].

ORTs are branching hyporeflective tubular structures with a hyper-reflective border. These represent areas of photoreceptor destruction and are irreversible.[34] The tubulations often overlie a fibrous scar and can be mistaken for intraretinal cystoid spaces. The presence of these findings serve as a negative biomarker in AMD treatment.[22]

Retinal pigment epithelial atrophy is identified on OCT by segments of enhanced signals beneath it.[32] It is a negative biomarker for eyes that have atrophy in the presence of active CNV at the start of anti-VEGF therapy. It is seen more commonly in eyes with Type 2 or 3 CNV. The rates of RPE atrophy were shown to be higher in eyes on monthly treatment with anti-VEGF agents in the CATT trial.[35]

External limiting membrane and ellipsoid layer integrity have been associated with good visual function in eyes with neovascular AMD.[36] The identification of these outer retinal layers is possible with newer SD-OCT systems.[10] However, their role in predicting visual outcomes after treatment is less well understood.

Choroidal thickness measurements are possible with the advent of enhanced depth imaging and SS imaging. Choroidal thickness reduces with advancing age. The role of choroidal thickness in neovascular AMD is unclear.[37] However, the diseases that come under the pachychoroid spectrum can often mimic neovascular AMD, and hence, the identification of an abnormally thick or thin choroid and detection of pachy vessels assumes importance.[38-40]

Vitreomacular interface

Posterior vitreous detachment has been identified as a positive biomarker in patients undergoing treatment for CNV. Eyes with a preexisting posterior vitreous detachment (PVD) have been shown to have a more benign course even with extended treatment intervals as opposed to patients with VMAs that require a more aggressive treatment protocol possibly including surgery.[41]

Optical Coherence Tomography in Macular Edema

Macular edema causing increased retinal thickness is a common consequence and cause of visual loss in a large number of retinal disorders, most often diabetic retinopathy, neovascular AMD and other causes of CNV, retinal vein occlusions (RVOs), hypertensive retinopathy, central serous chorioretinopathy (CSCR), Irvine–Gass syndrome, pars planitis and other uveitic entities, and retinitis pigmentosa. It may be secondary to traction such as with epiretinal membranes (ERMs) and VMT, drug-induced and overlying intraocular tumors as a sign of activity.[42,43] It is noted that fundus fluorescein angiography (FFA) leakage in CME is always associated with cystic changes on SD-OCT. Diffuse edema on FFA is more commonly associated with thickening and distortion of the retinal layers without cyst formation though rarely microcystoid changes may be seen on CME. Both situations, however, can coexist[44] Fig. 13 shows the various OCT findings in CME.

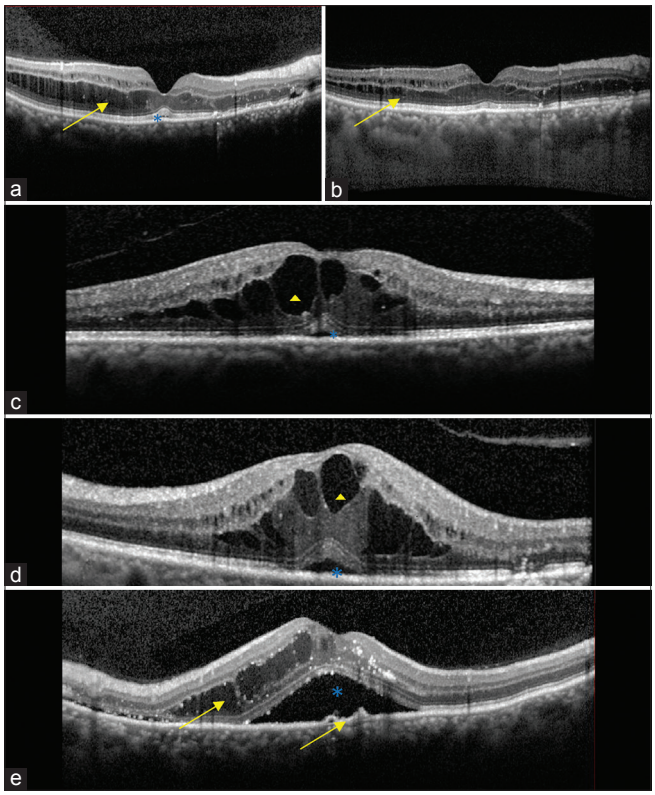

Figure 13: (a and b) Spectral domain optical coherence tomography pre- and post-treatment for diffuse diabetic macular edema. There is diffuse intraretinal fluid with cysts and schisis (yellow arrow). Both the thickening and the detachment are seen to reduce after intravitreal anti vascular endothelial growth factor injection. (c and d) Spectral domain optical coherence tomography images of varying severity of diabetic macular edema. Intraretinal cystic spaces are seen in the inner nuclear layer and Henle's layer (yellow arrowhead) with subfoveal detachment (blue star). (e) Spectral domain optical coherence tomography image of diabetic macular edema with diffuse retinal thickening (yellow arrow), intraretinal hyper reflective echoes and a significant amount of subretinal fluid (blue star). There is an area of irregularly elevated retinal pigment epithelium in the subfoveal region which showed a central serous chorioretinopathy leak on fundus fluorescein angiography (yellow arrow)

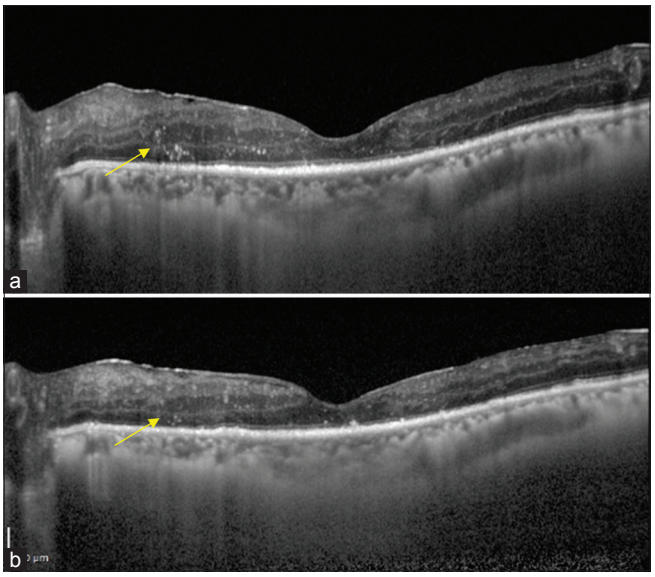

Figure 14: (a) Spectral domain optical coherence tomography of a patient with an epiretinal membrane and diffuse diabetic macular edema. Diffuse thickening of the Henle's layer is seen, with intraretinal hyper reflective deposits (yellow arrow). (b) Postantivascular endothelial growth factor injection, the epiretinal membrane is still seen on the surface, the retinal thickness and hyper reflective deposits have reduced (yellow arrow)

Irvine–Gass syndrome: Pseudophakic cystoid macular edema

In the early stages, the cystoid spaces are seen in the inner nuclear layer (INL), subsequently as severity increases, the outer plexiformlayer (OPL) is involved and in more severe cases, SRF is seen.[43,44]

Diabetic macular edema

Macular edema can present as diffuse retinal thickening, cystoid macular edema, tractional, and serous retinal detachment.[45,46] Diffuse edema is seen as reduced reflectivity of the OPL and INL with an increase in thickness, later on develops a spongy appearance. This is the earliest sign, is associated with good vision and responds best to treatment. CME is characterized by the accumulation of intraretinal fluid in well-defined spaces in the OPL. The arrangement of the Muller fibers as well as the orientation of the Henle's layer contributes to the characteristic appearance. Later, the cysts can coalesce to form larger cavities. The reflectivity of the content of the cysts as well as the size of the cysts is believed to have prognostic value.[47,48] Serous retinal detachment can occur in the chronic stages or if bilateral, could signify an underlying systemic complication such as nephropathy, multiple myeloma, etc., In contrast to serous retinal detachments which are convex, tractional detachments due to posterior hyaloid attachment and traction have a peaked configuration. OCT can detect macular edema that is not clinically evident, and several OCT-derived biomarkers are useful predictors of progression, severity, and visual outcome. These include retinal nerve fiber layer (RNFL) thickness, central subfield thickness, hyper reflective foci in the outer retina,[49] disorganization of the inner retinal layers DRIL[50] within a 1 mm zone centered on the fovea, ELM and ellipsoid zone disruption[49] and a newer biomarker "parallelism."[51] Figs. 14 and 15 show followup SD-OCT scans of diabetic macular edema (DME) showing reduction and worsening respectively.

Uveitic macular edema

Uveitic macular edema typically involves the INL though later such eyes show similar configuration on OCT as in DME with additional changes due to proliferative retinopathy, vasculitis, traction, or choroidal involvement.[52,53]

Macular edema in CNV

It can manifest either as intraretinal fluid, CME, SRF or RPE detachments. The presence of intra or SRF is an indication of activity that requires treatment. RPE detachments alone may not indicate the need for treatment. Cystoid changes can also be present over long-standing fibrotic lesions. The main role of OCT is to identify small changes in activity to determine the need to initiate, continue, stop, or switch treatment for CNV.[21,27,29,54,55]

Macular edema in retinal vein occlusions

This can present in the same way as DME except that the edema is usually segmental in a branch or tributary RVO. A higher

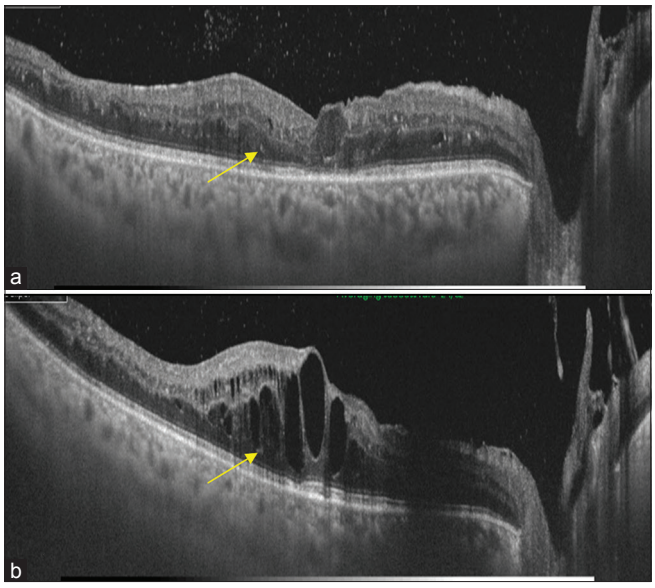

Figure 15: (a) Swept-source optical coherence tomography of diffuse diabetic macular edema showing intraretinal hyperreflective deposits and diffuse thickening of the Henle layer (yellow arrow). (b) Swept-source optical coherence tomography after 1 year showing an increase in the central retinal thickness along with prominent intraretinal cystic changes (yellow arrow)

incidence of serous retinal detachment is present in the acute phase and more of cystoid changes later. With increasing chronicity, schitic spaces may develop.[43,44,56]

Macular edema in tumors

SRF and CME can be seen on the surface of choroidal tumors and may cause a diagnostic dilemma if choroidal imaging is not performed.[57-59]

Common Errors in Interpretation of Macular Edema

Macular schisis

In patients with X-linked retinoschisis, the schisis cavity can occur in a number of different layers of the neurosensory retina (RNFL, INL, and ONL/outer plexiform layer). In CME, it predominantly involves the inner nuclear and outer plexiform layers.

Retinoschisis in optic pit

The schisis is seen to extend till the optic disc margin and involves the outer plexiform layer. The optic pit can be seen on OCT with a vitreous tuft that may be associated. However, the most common associated finding is serous retinal detachment with outer lamellar holes. Additional cystic changes may be seen in the inner layers. These changes are seen to reverse with the occurrence of PVD which could be spontaneous or surgical. However, VMT is typically absent.[13,42]

Myopic foveoschisis

The split is seen as vertical pillars rather than oval well-defined spaces. This can be seen in the inner, middle, or outer retinal layers with combinations of the same. Associated features in myopic eyes are ILM detachment, ERMs, retinal microfolds, ellipsoid zone defects, paravascularmicroholes

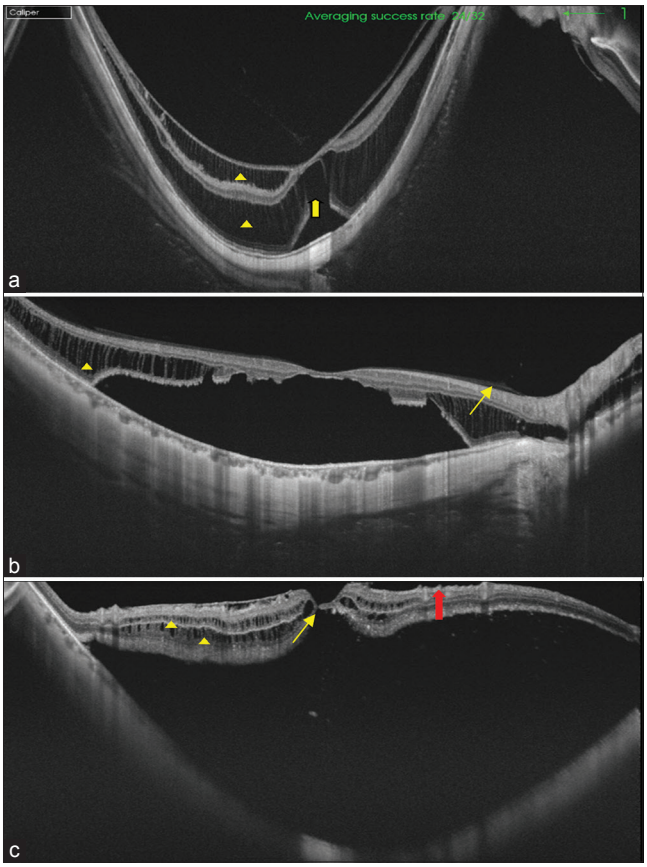

Figure 16: (a) Swept-source optical coherence tomography of a myopic staphyloma showing schisis in the inner and outer retinal layers (yellow triangle), as well as an outer retinal hole (yellow arrow). (b) Swept-source optical coherence tomography showing attached posterior hyaloid (yellow arrow) posterior pole neurosensory RD with outer layer schisis and coalescence of cavities (yellow triangle). (c) Swept-source optical coherence tomography showing posterior pole RD, inner and outer layer schisis (yellow arrow head) and a small full-thickness macular hole (yellow arrow) with epiretinal membrane (red arrow)

and macular holes, dome-shaped macula, and peripapillary intrachoroidal cavitations.[60-63] Evaluation of a myopic eye is best done with SS-OCT as it has a wider field and greater depth, enabling better imaging of deep posterior staphylomas [Fig. 16].

Outer retinal tubulation

ORT is seen as round or ovoid hyporeflective spaces with hyperreflective borders in the outer retina usually overlying areas of pigment epithelial atrophy or subretinal fibrosis. They are believed to represent degenerating photoreceptors and signify advanced disease. On cursory glance, they may appear as cystoid spaces, prompting unnecessary intervention as they have been shown to remain unchanged with treatment.[34]

As measurements of central retinal thickness are easily done, this is probably the most common parameter used to study treatment outcomes. However, the correlation between central retinal thickness and best-corrected visual acuity (BCVA) is seen to vary between conditions. A recent

analysis of clinical trial data of cases with neovascular AMD, DME, and RVO showed that at baseline, there was a small correlation between BCVA and central retinal thickness (CRT) in pooled AMD trial data, medium in pooled DME data and no correlation in pooled RVO data. At month 12, there was no correlation in AMD but medium correlation in DME and RVO data. Cases with recurrence in activity with shift to pro re nata (PRN) dosing showed correlation in AMD and RVO data. Overall, the best correlation was seen in DME indicating that in RVO and AMD, the relationship may be dependent on other factors as well.[24]

Optical Coherence Tomography in Conditions Causing Serous Detachment at the Macula

Common conditions that cause serous detachment at the macula include CSCR, age-related macular degeneration, PCV, CNV complicating CSCR, pachychoroid neovasculopathy (Type 1 CNV with pachychoroid), dome-shaped macula with subfoveal detachment, optic disc pit, lupus erythematosus, choroidal ischemic disorders such as accelerated hypertension and preeclampsia, systemic corticosteroid usage, paraproteinemia, choroidal tumors, and in inflammatory disorders such as Harada's disease.[64,65]

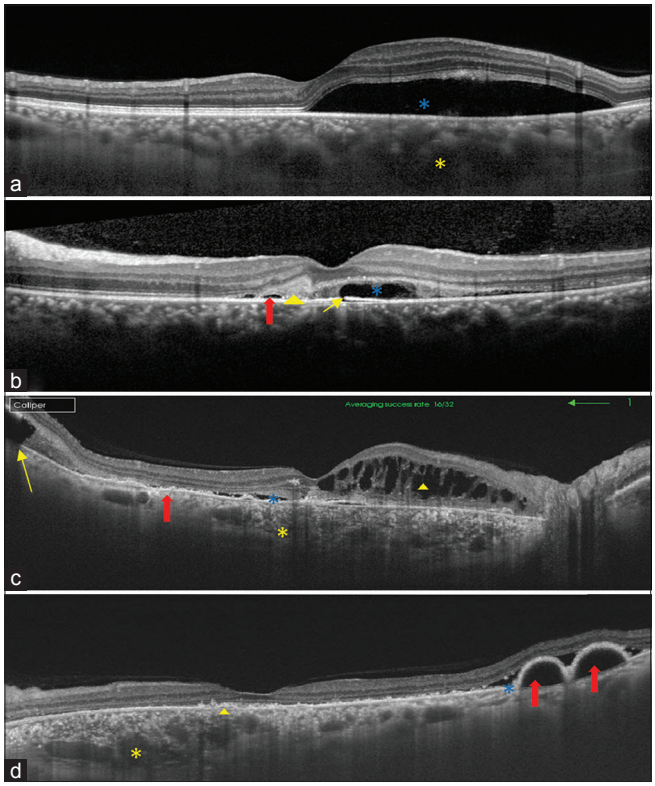

Figure 17: (a) Central serous chorioretinopathy with neurosensory RD, low-reflective subretinal deposits (blue star), and dilated large choroidal vessels (yellow star). (b) Fibrinous central serous chorioretinopathy with subfoveal neurosensory RD (blue star), subretinal fibrin (yellow triangle) that overlies a pigment epithelial detachment (red arrow) with subfoveal microrip (yellow arrow). (c and d) Bilateral chronic central serous chorioretinopathy and pachychoroid. Both eyes show intraretinal cystoid spaces (yellow triangle), shallow subretinal fluid (blue star), irregular retinal pigment epithelium elevation and dilated large choroidal vessels (yellow star), retinal pigment epithelium rip in the right eye (yellow arrow) and two serous pigment epithelial detachments (red arrows) in the left

Central serous chorioretinopathy

The characteristic OCT appearance is a localized detachment of the neurosensory retina typically at the macula.

The detached retina may be normal in acute cases; show intraretinal hyperreflective deposits in the ONL, OPL, ELM, and ellipsoid zone in chronic or recurrent cases; and may show thinning of the ONL, disruption of ELM, and ellipsoid zone in chronic cases.[66] Cystoid changes are a feature of chronicity[54] and may be seen in cases of more than 5 years duration.

The detached retina shows elongated photoreceptor segments which are a feature of most acute cases.[67] Subretinal hyperreflective deposits may be seen in long-standing cases and suggest a lower final visual acuity. The subretinal space may show moderate or highly reflective homogenous areas suggestive of fibrin with characteristic areas of clearing within them.[68,69]

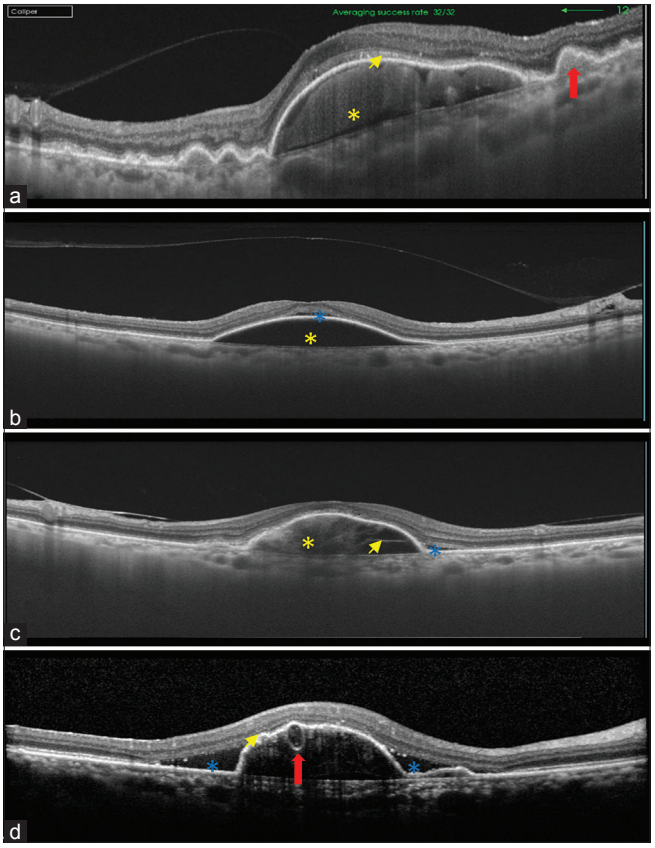

Figure 18: (a) Drusenoid pigment epithelial detachment in age-related macular degeneration with homogenous content (yellow star) and soft drusen (red arrow). Intraretinal hyperreflective dots are seen (yellow arrow). (b) Smooth, dome-shaped, high-reflective serous pigment epithelial detachment with clear subretinal pigment epithelium space (yellow star) and a small pocket of subretinal fluid over the summit (blue star). (c) Fibrovascular pigment epithelial detachment with irregular retinal pigment epithelium elevation and heterogeneous content (yellow star). Moderately reflective subretinal pigment epithelium vascular structures (yellow arrow) and subretinal fluid (blue star). (d) Pigment epithelial detachment in polypoidal choroidal vasculopathy with irregularly elevated retinal pigment epithelium (yellow arrow), subretinal fluid (blue star), and subretinal pigment epithelium polyps (red arrow)

The pigment epithelium may show single or multiple serous PEDs which could be a feature of acute, chronic, or inactive disease, microrips of the RPE[70] which suggest an active episode, RPE hypertrophy, or atrophy which are seen in chronic CSCR. The area of active leak may be seen either as a PED with a microrip, an area of RPE elevation or may be indicated by a sagging of the posterior layers of the detached retina toward an area of RPE elevation or detachment.[68] The bullous variant shows large RPE rips.[71]

Choroidal imaging of almost all eyes with active CSCR as well as some asymptomatic fellow eyes shows subfovealchoroidal thickening and dilated choroidal vessels.[72] Chronic CSCR is believed to be part of the pachychoroid spectrum. Other features described include thinning of the inner choroidal vessels, focal choroidal excavation[73-75] (defined as a macular lesion with choroidal excavation detected on SD-OCT without evidence of scleral ectasia or posterior staphyloma), and loculation of fluid in the posterior choroid.[76] Fig. 17 shows the various OCT manifestations of CSCR.

Optical coherence tomography in Vogt-Koyanagi-Harada versus central serous chorioretinopathy

Common features are serous macular detachments and choroidal thickening. Features associated with CSCR are PED, Microrips of the RPE, RPE irregularity, fibrin with areas of echo lucency and large choroidal vessel dilatation. Features more suggestive of Vogt-Koyanagi-Harada (VKH) are subretinal septae, multiple pockets of SRF, RPE undulations, ILM irregularities and loss of reflectivity in the inner choroid, gross choroidal thickening with inability to visualize the choroidoscleral junction.[77-79]

Retinal Pigment Epithelial Detachments

Fig. 18 shows the OCT images of various types of PED.

Drusenoid pigment epithelial detachment

Drusenoid PEDs are a component of high risk AMD. They are seen as high reflective smooth or undulating elevations of the RPE . The sub RPE material is dense , homogeneous and of moderate to high reflectivity. Hyper reflective foci above the RPE indicate pigmentation. A small pocket of SRF over the PED is insignificant. Signs of associated CNV are intraretinal and/or SRF, heterogenous, or hyporeflective sub-RPE content.[31]

Serous pigment epithelial detachment

Well-demarcated highly reflective elevations of the RPE with the sub-RPE space being hyporeflective or optically empty. Long-standing cases may have hyperreflective foci on the surface indicating pigment clumping. Heterogeneous content of the PED indicates the presence of associated CNV.[31] Serous PED in CSCR is usually associated with underlying thickened choroid but may not be so in AMD.[64]

Fibrovascular pigment epithelial detachment (vascularized pigment epithelial detachment) or Type 1 choroidal neovascularization

The content of the PED is either solid with lamellar structures and clefts or hyperreflective material stuck along the undersurface. Layered hyperreflective bands may be seen "the onion sign" - indicative of lipid exudation under the PED.[80]

Pigment epithelial detachment in polypoidal choroidal vasculopathy

Typically, hemorrhagic, serous, or a combination of the two, hemorrhagic PED is characterized by a very highly reflective thick elevation of the RPE with intense shadowing obscuring the details below it. The vascular complex or polyps can sometimes be seen as round or ovoid structures with variable hyporeflectivity in the center and a hyperreflective wall, on the undersurface of the PED. Occasionally, the polyp is seen to erode through the RPE into the subretinal space. SRF may be associated. The "triple layer sign" originally described in PCV but no longer considered pathognomonic consists of a triad of a PED, the lamellar scar and a second hyporeflective space or cleft is visualized immediately under it.[81]

Pigment epithelial detachment in Type 3 choroidal neovascularization or retinal angiomatous proliferation

OCT features are seen both above and below the RPE, which may be develop either simultaneously or sequentially in the course of progression. The evolution of the lesion has been described in three stages with typical OCT features which include a subtle irregular elevation of the RPE (erosion sign) or a frank PED associated with a localized discontinuity in the RPE (flap sign) through which a tubular continuous structure may be seen connecting the pre- and sub-RPE space and a focal funnel-shaped RPE joining an inverted funnel-shaped inner neuroepithelium ("kissing sign") over a large serosanguineous PED. The area over the PED may show ELM disruption, intraretinal edema, and CME, which is helps to differentiate Type 2 from Type 3 CNV.[82]

Pigment epithelial detachments in central serous chorioretinopathy

PEDs in CSCR, systemic conditions such as paraproteinemias, renal disease, inflammations, typically have a serous appearance.[65] Choroidal imaging and systemic evaluation help in the differentiation. PEDs in lymphomas have a high-reflective sub-RPE space.

Retinal pigment epithelium rip

Large PEDs with height >600 μ, diameter >5 mm are at risk of RPE tears. Signs of an impending rip in FVPED are folding and corrugation of the RPE with flattening of the PED because of contracture of the sub-PED neovascular membrane.[31]

Choroidal Imaging

In conventional SD-OCT imaging systems, it is possible to image the choroid by shifting the zero delay line or point of highest sensitivity from its conventional location, more posteriorly toward the sclera. This technique called enhanced-depth imaging or EDI-OCT enables an overall assessment of the choroid and the choroidoscleral interface.[83] However, this technique does not significantly visualize the choriocapillaris or the choroidal microvasculature which are in close proximity to the RPE. The advantages of SS-OCT technology are higher imaging speed; higher detection efficiencies, improved imaging range, and reduced sensitivity roll off with increasing depth. These enable a better imaging of the internal structure of the choroid including the choriocapillaris and the choroidoscleral interface which is further enhanced by generating en face images as part of postacquisition image processing.[84,85]

The total choroidal thickness is defined as the distance between the outer aspect of the hyperreflective layer that corresponds to the RPE/Bruch membrane complex and the choroidoscleral interface.[84] The subfoveal choroidal thickness measurement though possible once the interfaces are identified is often a challenge. This is due to the high degree of variability in measurements even in normal subjects that includes variations with gender, age, race, refractive error, axial lengths, diurnal variation, and even the degree of accommodation.[86,87]

Differentiating the individual layers is not easy. The choriocapillaris is normally very strongly adherent to the Bruch's membrane. The extremely thin-walled nature and density again makes identification difficult though most suggest that it is represented by hyperreflective dots beneath the Bruch's membrane – RPE complex. Differentiation between the choriocapillaris and medium sized choroidal vessels is again difficult, but the larger choroidal vessels are easier to identify. As a general guide, the choriocapillaris is identified as a thin layer of moderate reflectivity in the space just adjacent to the RPE-Bruch's complex. The layer of medium choroidal vessels (Sattler's layer) is seen as a thick layer of round or oval hyporeflective spaces with hyperreflective margins in the middle choroid whereas the Haller's layer of large choroidal vessels is formed by larger oval hyporeflective spaces in the outer choroid adjacent to the homogenous band that represents the choroidoscleral interface.[10]

Noninvasive choroidal imaging with OCT has increased our understanding of the role of the choroid in various disease conditions.

Age-related macular degeneration

In eyes with early or intermediate AMD, no consistent choroidal thickness abnormalities have been noted, but many studies have shown thinning of the choroid in eyes with advanced AMD compared to age-matched controls. However, in eyes with reticular pseudodrusen, diffuse choroidal thinning, and lack of choriocapillaris has been demonstrated, as also in a newly described entity called age-related choroidal atrophy.[88]

Polypoidal choroidal vasculopathy

The subfoveal total choroidal thickness is increased in PCV, compared to typical AMD, in both affected and asymptomatic contralateral eyes, even after adjustment for age, gender, and refractive error.[37] However, a recent study has shown a subset of eyes with typical PCV having a normal or thinner than normal choroid.

Central serous chorioretinopathy

The role of the choroid is being increasingly noted in this condition with the subfoveal total choroidal thickness being increased almost universally in CSCR.[64] It is seen to be thickened in even the apparently uninvolved fellow eye in some series. Focal or diffuse dilatation of the choroidal vessels has also been seen on enface OCT images though its exact relevance remains unclear. Thickness of the choroid is seen to reduce with treatments such as photodynamic therapy (PDT), oral acetazolamide, and anti-VEGF agents, but the thickness always remains above normal.

Pachychoroid

This is a relatively recently described entity characterized by an abnormal and permanent increase in choroidal thickness, associated with dilated choroidal vessels and other structural alterations of the normal choroidal architecture. The spectrum includes pachychoroid pigment epitheliopathy, CSCR, pachychoroid neovasculopathy, and PCV.[38-40] Typically, the larger choroidal vessels are dilated, and in these areas, the choriocapillaries and Sattler's layer are compressed or obliterated. The overlying RPE may show irregularities, a Type 1 CNV or polypoidal lesion may be seen.

Uveitis

EDI and SS-OCT imaging has generated a better understanding of choroidal changes in eyes with posterior uveitis.[89,90]

In the acute phase of VKH, the subfoveal choroid is seen to be diffusely thickened with loss of the hyperreflective dots in the inner choroid that indicates inflammation.[79] The RPE layer can appear to have a bumpy surface, especially in eyes with severe exudative retinal detachment (RD). Occasionally, the thickening of the choroid is so significant that the choroidoscleral junction is not apparent. However, with initiation of treatment, the choroidal thickness is seen to reduce. In eyes with chronic disease and depigmentation, the choroid is significantly thinner than normal. A more significant use of choroidal imaging is the detection of choroidal thickening in an eye that appears to be in the quiescent stage.[91] This finding suggests persistent subclinical inflammation and warrants additional investigations. It has also be shown to detect rebound choroidal thickness described as an increase of more than 100 microns in the absence of other clinical signs of inflammation [Fig. 19].

Eyes with birdshot chorioretinopathy and Behcet's disease have choroidal thinning.[92,93]

Choroidal imaging has made it possible to characterize choroidal granulomas which are seen as localized low-reflective areas within the choroid. Serial OCTs can be used to monitor the response to therapy.[94,95]

In eyes with posterior scleritis, the choroid may be significantly thickened and it may be difficult to visualize

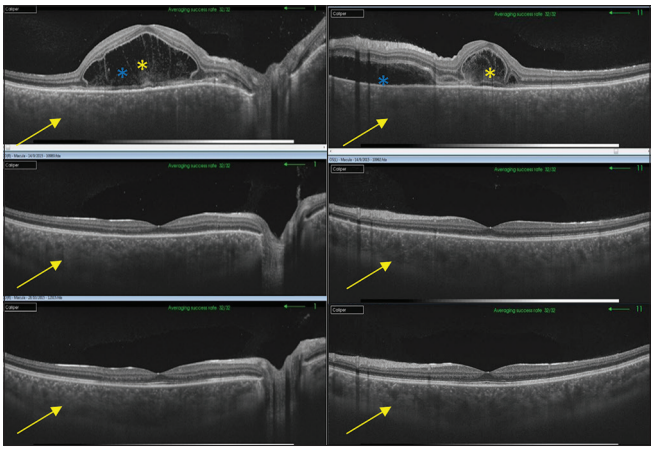

Figure 19: Swept-source optical coherence tomography of bilateral Vogt-Koyanagi-Harada at presentation and two follow-up visits. The topmost set of images shows the typical feature of subretinal fluid (blue star) with multiple septae signifying fibrin (yellow star). The choroid shows thickening, high-reflective infiltrates, and loss of the sclerochoroidal demarcation line (yellow arrow). The middle and bottom images show dramatic resolution of the subretinal fluid with treatment but persistent choroidal thickening that signifies subclinical activity (yellow arrow). The patient had a recurrence of symptoms after 4 months

the choroidoscleral junction in the acute phase, but with repeated episodes of scleritis, significant thinning of the choroid is seen.

Choroidal and retinal tumors

EDI and SS-OCT give valuable information in retinal and small choroidal tumors that cannot be characterized on conventional ultrasound. In addition to overlying retinal changes that are secondary to the tumor, the surface as well as intralesional characteristics of most of the common retinal and choroidal tumors are better understood.[57-59]

Contour abnormalities of the choroid and sclera are well seen using EDI and SS OCT, and even more so in high myopia where the penetration is deeper due to the thinner choroid and relatively depigmented RPE. These include posterior staphyloma,[96-98] dome-shaped macula.[60,99-101] peripapillary and macular intrachoroidal cavitations,[61,62] and optic pits and colobomas[102-104]

Table 5 is a short summary of the steps involved in the interpretation of an image on OCT.

Conclusion

OCT is a noninvasive, quick, and reproducible investigation that has revolutionized the imaging of posterior segment lesions. Correlation of individual layers involved on OCT with histopathology has brought us much closer to an accurate tissue diagnosis than ever before. Various combinations of findings on OCT and comparison with known OCT-based biomarkers have made disease identification and prognostication much simpler. The development of standardized protocols for imaging and measuring specific areas and software to ensure repeated evaluation of the same point at different time frames, it is possible to collect and reliably evaluate large data for multicentric trials. Automated image analysis of known OCT biomarkers for AMD is aimed at simplifying quantification of these biomarkers, thereby helping in grading of large data.[105]

Newer developments with the technology include intraoperative OCT,[106,107] ultra-wide field OCT,[108] OCT Angiography and its newer algorithms including optical microangiography, speckle variance, phase variance, split-spectrum amplitude-decorrelation angiography, and correlation mapping,[109] and adaptive optics OCT.[110] These would further enhance understanding of both anatomical and functional aspects of retinal pathology.

Table 5: Ten steps toward interpretation of an optical coherence tomography image

1. Determine the indication for the OCT from the patient's record, fundus pictures, angiograms, etc., Does the OCT image show the area of interest?
2. Is the scan protocol used appropriate for the information required?
3. Is the scan quality good enough for analysis? Identify artifacts, other findings that could affect image quality
4. Use the Macular cube, 3D, or volume scans for evaluation of the pathology in toto, including the segment maps. Color or grayscale images are both adequate
5. Look at the macular thickness map and ETDRS grid and get an idea as to the location of the pathology. Ensure that the overlay of the thickness map is centered on the fovea in the color, SLO, or IR image
6. Evaluate each layer from the posterior vitreous to the choroidoscleral junction if visible, for deviation from the normal. The HD 5 line raster scans or line scans are preferable for this as they scan a precise location and have a higher resolution. Grayscale images are preferable
7. Classify the abnormality into one or more of the following: change in contour, change in thickness, change in reflectivity, loss of tissue, presence of abnormal tissue. Look for the location of the abnormality, layers involved either primarily or as part of secondary effects
8. Take measurements as appropriate in addition to the standard thickness measurements that are inbuilt in the protocols. In case of follow-up scans, use software to analyze change
9. Advanced analysis such as en face OCT images can be generated in selected instances
10. Look for the presence of known biomarkers before making the final diagnosis

OCT: Optical coherence tomography, ETDRS: Early treatment diabetic retinopathy study, SLO: Scanning laser ophthalmoscopy, HD: High definition, 3D: Three-dimensional, IR: Infrared

Acknowledgments

The authors would like to acknowledge the contribution of the departments of optometry, photography, uveitis and Shri Bhagwan Mahavir VR Services

Financial support and sponsorship

Nil.

Conflicts of interest

There are no conflicts of interest.

References

1. Huang D, Swanson EA, Lin CP, Schuman JS, Stinson WG, Chang W, *et al*. Optical coherence tomography. Science 1991;254:1178-81.
2. Diabetic Retinopathy Clinical Research Network Writing Committee, Bressler SB, Edwards AR, Chalam KV, Bressler NM, Glassman AR, *et al.* Reproducibility of spectral-domain optical coherence tomography retinal thickness measurements and conversion to equivalent time-domain metrics in diabetic macular edema. JAMA Ophthalmol 2014;132:1113-22.
3. Diabetic Retinopathy Clinical Research Network, Browning DJ, Glassman AR, Aiello LP, Beck RW, Brown DM, *et al.* Relationship between optical coherence tomography-measured central retinal thickness and visual acuity in diabetic macular edema. Ophthalmology 2007;114:525-36.
4. Wolf-Schnurrbusch UE, Ceklic L, Brinkmann CK, Iliev ME, Frey M, Rothenbuehler SP, *et al.* Macular thickness measurements in healthy eyes using six different optical coherence tomography instruments. Invest Ophthalmol Vis Sci 2009;50:3432-7.
5. Girkin CA, McGwin G Jr. Sinai MJ, Sekhar GC, Fingeret M, Wollstein G, *et al.* Variation in optic nerve and macular structure with age and race with spectral-domain optical coherence tomography. Ophthalmology 2011;118:2403-8.
6. Browning DJ, Glassman AR, Aiello LP, Bressler NM, Bressler SB, Danis RP, *et al.* Optical coherence tomography measurements and analysis methods in optical coherence tomography studies of diabetic macular edema. Ophthalmology 2008;115:1366-71, 1371.e1.
7. Giani A, Cigada M, Esmaili DD, Salvetti P, Luccarelli S, Marziani E, *et al.* Artifacts in automatic retinal segmentation using different optical coherence tomography instruments. Retina 2010;30:607-16.
8. Domalpally A, Danis RP, Zhang B, Myers D, Kruse CN. Quality

issues in interpretation of optical coherence tomograms in macular diseases. Retina 2009;29:775-81.

9. Han IC, Jaffe GJ. Evaluation of artifacts associated with macular spectral-domain optical coherence tomography. Ophthalmology 2010;117:1177-89.
10. Staurenghi G, Sadda S, Chakravarthy U, Spaide RF, International Nomenclature for Optical Coherence Tomography (IN•OCT) Panel. Proposed lexicon for anatomic landmarks in normal posterior segment spectral-domain optical coherence tomography: The IN•OCT consensus. Ophthalmology 2014;121:1572-8.
11. Duker JS, Kaiser PK, Binder S, de Smet MD, Gaudric A, Reichel E, *et al.* The international vitreomacular traction study group classification of vitreomacular adhesion, traction, and macular hole. Ophthalmology 2013;120:2611-9.
12. Koizumi H, Spaide RF, Fisher YL, Freund KB, Klancnik JM Jr., Yannuzzi LA, *et al.* Three-dimensional evaluation of vitreomacular traction and epiretinal membrane using spectral-domain optical coherence tomography. Am J Ophthalmol 2008;145:509-17.
13. Mirza RG, Johnson MW, Jampol LM. Optical coherence tomography use in evaluation of the vitreoretinal interface: A review. Surv Ophthalmol 2007;52:397-421.
14. Ip MS, Baker BJ, Duker JS, Reichel E, Baumal CR, Gangnon R, *et al.* Anatomical outcomes of surgery for idiopathic macular hole as determined by optical coherence tomography. Arch Ophthalmol 2002;120:29-35.
15. Androudi S, Stangos A, Brazitikos PD. Lamellar macular holes: Tomographic features and surgical outcome. Am J Ophthalmol 2009;148:420-6.
16. Allen AW Jr., Gass JD. Contraction of a perifoveal epiretinal membrane simulating a macular hole. Am J Ophthalmol 1976;82:684-91.
17. Gass JD. Biomicroscopic and histopathologic considerations regarding the feasibility of surgical excision of subfoveal neovascular membranes. Am J Ophthalmol 1994;118:285-98.
18. Regatieri CV, Branchini L, Duker JS. The role of spectral-domain OCT in the diagnosis and management of neovascular age-related macular degeneration. Ophthalmic Surg Lasers Imaging 2011;42 Suppl:S56-66.
19. Lim EH, Han JI, Kim CG, Cho SW, Lee TG. Characteristic findings of optical coherence tomography in retinal angiomatous proliferation. Korean J Ophthalmol 2013;27:351-60.
20. Freund KB, Ho IV, Barbazetto IA, Koizumi H, Laud K, Ferrara D, *et al.* Type 3 neovascularization: The expanded spectrum of retinal angiomatous proliferation. Retina 2008;28:201-11.
21. Freund KB, Zweifel SA, Engelbert M. Do we need a new classification for choroidal neovascularization in age-related macular degeneration? Retina 2010;30:1333-49.
22. Schmidt-Erfurth U, Waldstein SM. A paradigm shift in imaging biomarkers in neovascular age-related macular degeneration. Prog Retin Eye Res 2016;50:1-24.
23. Phadikar P, Saxena S, Ruia S, Lai TY, Meyer CH, Eliott D, *et al.* The potential of spectral domain optical coherence tomography imaging based retinal biomarkers. Int J Retina Vitreous 2017;3:1.
24. Ou WC, Brown DM, Payne JF, Wykoff CC. Relationship between visual acuity and retinal thickness during anti-vascular endothelial growth factor therapy for retinal diseases. Am J Ophthalmol 2017;180:8-17.
25. Holz FG, Amoaku W, Donate J, Guymer RH, Kellner U, Schlingemann RO, *et al.* Safety and efficacy of a flexible dosing regimen of ranibizumab in neovascular age-related macular degeneration: The SUSTAIN study. Ophthalmology 2011;118:663-71.
26. Fung AE, Lalwani GA, Rosenfeld PJ, Dubovy SR, Michels S, Feuer WJ, *et al.* An optical coherence tomography-guided, variable dosing regimen with intravitreal ranibizumab (Lucentis) for neovascular age-related macular degeneration. Am J Ophthalmol 2007;143:566-83.
27. Schmidt-Erfurth U, Chong V, Loewenstein A, Larsen M, Souied E, Schlingemann R, *et al.* Guidelines for the management of neovascular age-related macular degeneration by the European Society of Retina Specialists (EURETINA). Br J Ophthalmol 2014;98:1144-67.
28. Simader C, Ritter M, Bolz M, Deák GG, Mayr-Sponer U, Golbaz I, *et al.* Morphologic parameters relevant for visual outcome during anti-angiogenic therapy of neovascular age-related macular degeneration. Ophthalmology 2014;121:1237-45.
29. Waldstein SM, Wright J, Warburton J, Margaron P, Simader C, Schmidt-Erfurth U, *et al.* Predictive value of retinal morphology for Visual acuity outcomes of different ranibizumab treatment regimens for neovascular AMD. Ophthalmology 2016;123:60-9.
30. Querques G, Coscas F, Forte R, Massamba N, Sterkers M, Souied EH, *et al.* Cystoid macular degeneration in exudative age-related macular degeneration. Am J Ophthalmol 2011;152:100-700.
31. Mrejen S, Sarraf D, Mukkamala SK, Freund KB. Multimodal imaging of pigment epithelial detachment: A guide to evaluation. Retina 2013;33:1735-62.
32. Keane PA, Patel PJ, Liakopoulos S, Heussen FM, Sadda SR, Tufail A, *et al.* Evaluation of age-related macular degeneration with optical coherence tomography. Surv Ophthalmol 2012;57:389-414.
33. Christenbury JG, Folgar FA, O'Connell RV, Chiu SJ, Farsiu S, Toth CA, *et al.* Progression of intermediate age-related macular degeneration with proliferation and inner retinal migration of hyperreflective foci. Ophthalmology 2013;120:1038-45.
34. Zweifel SA, Engelbert M, Laud K, Margolis R, Spaide RF, Freund KB, *et al.* Outer retinal tubulation: A novel optical coherence tomography finding. Arch Ophthalmol 2009;127:1596-602.
35. Ying GS, Kim BJ, Maguire MG, Huang J, Daniel E, Jaffe GJ, *et al.* Sustained visual acuity loss in the comparison of age-related macular degeneration treatments trials. JAMA Ophthalmol 2014;132:915-21.
36. Kim YM, Kim JH, Koh HJ. Improvement of photoreceptor integrity and associated visual outcome in neovascular age-related macular degeneration. Am J Ophthalmol 2012;154:164-730.
37. Chung SE, Kang SW, Lee JH, Kim YT. Choroidal thickness in polypoidal choroidal vasculopathy and exudative age-related macular degeneration. Ophthalmology 2011;118:840-5.
38. Lehmann M, Bousquet E, Beydoun T, Behar-Cohen F. PACHYCHOROID: An inherited condition? Retina 2015;35:10-6.
39. Pang CE, Freund KB. Pachychoroid neovasculopathy. Retina 2015;35:1-9.
40. Warrow DJ, Hoang QV, Freund KB. Pachychoroid pigment epitheliopathy. Retina 2013;33:1659-72.
41. Mayr-Sponer U, Waldstein SM, Kundi M, Ritter M, Golbaz I, Heiling U, *et al.* Influence of the vitreomacular interface on outcomes of ranibizumab therapy in neovascular age-related macular degeneration. Ophthalmology 2013;120:2620-9.
42. Trichonas G, Kaiser PK. Optical coherence tomography imaging of macular oedema. Br J Ophthalmol 2014;98 Suppl 2:ii24-9.
43. Catier A, Tadayoni R, Paques M, Erginay A, Haouchine B, Gaudric A, *et al.* Characterization of macular edema from various etiologies by optical coherence tomography. Am J Ophthalmol 2005;140:200-6.
44. Brar M, Yuson R, Kozak I, Mojana F, Cheng L, Bartsch DU, *et al.* Correlation between morphologic features on spectral-domain optical coherence tomography and angiographic leakage patterns in macular edema. Retina 2010;30:383-9.
45. Otani T, Kishi S, Maruyama Y. Patterns of diabetic macular edema with optical coherence tomography. Am J Ophthalmol 1999;127:688-93.

46. Kim BY, Smith SD, Kaiser PK. Optical coherence tomographic patterns of diabetic macular edema. Am J Ophthalmol 2006;142:405-12.
47. Horii T, Murakami T, Nishijima K, Akagi T, Uji A, Arakawa N, *et al.* Relationship between fluorescein pooling and optical coherence tomographic reflectivity of cystoid spaces in diabetic macular edema. Ophthalmology 2012;119:1047-55.
48. Horii T, Murakami T, Akagi T, Uji A, Ueda-Arakawa N, Nishijima K, *et al.* Optical coherence tomographic reflectivity of cystoid spaces is related to recurrent diabetic macular edema after triamcinolone. Retina 2015;35:264-71.
49. Uji A, Murakami T, Nishijima K, Akagi T, Horii T, Arakawa N, *et al.* Association between hyperreflective foci in the outer retina, status of photoreceptor layer, and visual acuity in diabetic macular edema. Am J Ophthalmol 2012;153:710-7, 717.e1.
50. Radwan SH, Soliman AZ, Tokarev J, Zhang L, van Kuijk FJ, Koozekanani DD, *et al.* Association of disorganization of retinal inner layers with vision after resolution of center-involved diabetic macular edema. JAMA Ophthalmol 2015;133:820-5.
51. Uji A, Murakami T, Unoki N, Ogino K, Horii T, Yoshitake S, *et al.* Parallelism for quantitative image analysis of photoreceptor-retinal pigment epithelium complex alterations in diabetic macular edema. Invest Ophthalmol Vis Sci 2014;55:3361-7.
52. Markomichelakis NN, Halkiadakis I, Pantelia E, Peponis V, Patelis A, Theodossiadis P, *et al.* Patterns of macular edema in patients with uveitis: Qualitative and quantitative assessment using optical coherence tomography. Ophthalmology 2004;111:946-53.
53. Tran TH, de Smet MD, Bodaghi B, Fardeau C, Cassoux N, Lehoang P, *et al.* Uveitic macular oedema: Correlation between optical coherence tomography patterns with visual acuity and fluorescein angiography. Br J Ophthalmol 2008;92:922-7.
54. Iida T, Yannuzzi LA, Spaide RF, Borodoker N, Carvalho CA, Negrao S, *et al.* Cystoid macular degeneration in chronic central serous chorioretinopathy. Retina 2003;23:1-7.
55. Schmidt-Erfurth U, Waldstein SM, Deak GG, Kundi M, Simader C. Pigment epithelial detachment followed by retinal cystoid degeneration leads to vision loss in treatment of neovascular age-related macular degeneration. Ophthalmology 2015;122:822-32.
56. Spaide RF, Lee JK, Klancnik JK Jr., Gross NE. Optical coherence tomography of branch retinal vein occlusion. Retina 2003;23:343-7.
57. Shields CL, Manalac J, Das C, Saktanasate J, Shields JA. Review of spectral domain enhanced depth imaging optical coherence tomography of tumors of the choroid. Indian J Ophthalmol 2015;63:117-21.
58. Shields CL, Manalac J, Das C, Saktanasate J, Shields JA. Review of spectral domain-enhanced depth imaging optical coherence tomography of tumors of the retina and retinal pigment epithelium in children and adults. Indian J Ophthalmol 2015;63:128-32.
59. Shields CL, Pellegrini M, Ferenczy SR, Shields JA. Enhanced depth imaging optical coherence tomography of intraocular tumors: From placid to seasick to rock and rolling topography – the 2013 Francesco Orzalesi lecture. Retina 2014;34:1495-512.
60. Imamura Y, Iida T, Maruko I, Zweifel SA, Spaide RF. Enhanced depth imaging optical coherence tomography of the sclera in dome-shaped macula. Am J Ophthalmol 2011;151:297-302.
61. Spaide RF, Akiba M, Ohno-Matsui K. Evaluation of peripapillary intrachoroidal cavitation with swept source and enhanced depth imaging optical coherence tomography. Retina 2012;32:1037-44.
62. Ohno-Matsui K, Akiba M, Moriyama M, Ishibashi T, Hirakata A, Tokoro T, *et al.* Intrachoroidal cavitation in macular area of eyes with pathologic myopia. Am J Ophthalmol 2012;154:382-93.
63. Gohil R, Sivaprasad S, Han LT, Mathew R, Kiousis G, Yang Y, *et al.* Myopic foveoschisis: A clinical review. Eye (Lond) 2015;29:593-601.
64. Daruich A, Matet A, Dirani A, Bousquet E, Zhao M, Farman N, *et al.* Central serous chorioretinopathy: Recent findings and new physiopathology hypothesis. Prog Retin Eye Res 2015;48:82-118.
65. Marmor M. On the cause of serous detachments and acute central serous chorioretinopathy. Br J Ophthalmol 1997;81:812-3.
66. Ahlers C, Geitzenauer W, Stock G, Golbaz I, Schmidt-Erfurth U, Prünte C, *et al.* Alterations of intraretinal layers in acute central serous chorioretinopathy. Acta Ophthalmol 2009;87:511-6.
67. Matsumoto H, Kishi S, Otani T, Sato T. Elongation of photoreceptor outer segment in central serous chorioretinopathy. Am J Ophthalmol 2008;145:162-8.
68. Fujimoto H, Gomi F, Wakabayashi T, Sawa M, Tsujikawa M, Tano Y, *et al.* Morphologic changes in acute central serous chorioretinopathy evaluated by fourier-domain optical coherence tomography. Ophthalmology 2008;115:1494-500, 1500.e1-2.
69. Yannuzzi NA, Mrejen S, Capuano V, Bhavsar KV, Querques G, Freund KB, *et al.* A central hyporeflective subretinal lucency correlates with a region of focal leakage on fluorescein angiography in eyes with central serous chorioretinopathy. Ophthalmic Surg Lasers Imaging Retina 2015;46:832-6.
70. Yang L, Jonas JB, Wei W. Optical coherence tomography-assisted enhanced depth imaging of central serous chorioretinopathy. Invest Ophthalmol Vis Sci 2013;54:4659-65.
71. Balaratnasingam C, Freund KB, Tan AM, Mrejen S, Hunyor AP, Keegan DJ, *et al.* Bullous variant of central serous chorioretinopathy: Expansion of phenotypic features using multimethod imaging. Ophthalmology 2016;123:1541-52.
72. Chen G, Tzekov R, Li W, Jiang F, Mao S, Tong Y, *et al.* Subfoveal choroidal thickness in central serous chorioretinopathy: A Meta-analysis. PLoS One 2017;12:e0169152.
73. Lee CS, Woo SJ, Kim YK, Hwang DJ, Kang HM, Kim H, *et al.* Clinical and spectral-domain optical coherence tomography findings in patients with focal choroidal excavation. Ophthalmology 2014;121:1029-35.
74. Chung H, Byeon SH, Freund KB. Focal choroidal excavation and its association with pachychoroid spectrum disorders: A Review of the literature and multimodal imaging findings. Retina 2017;37:199-221.
75. Margolis R, Mukkamala SK, Jampol LM, Spaide RF, Ober MD, Sorenson JA, *et al.* The expanded spectrum of focal choroidal excavation. Arch Ophthalmol 2011;129:1320-5.
76. Spaide RF, Ryan EH Jr. Loculation of fluid in the posterior choroid in eyes with central serous chorioretinopathy. Am J Ophthalmol 2015;160:1211-6.
77. Fong AH, Li KK, Wong D. Choroidal evaluation using enhanced depth imaging spectral-domain optical coherence tomography in Vogt-Koyanagi-Harada disease. Retina 2011;31:502-9.
78. Lin D, Chen W, Zhang G, Huang H, Zhou Z, Cen L, *et al.* Comparison of the optical coherence tomographic characters between acute Vogt-Koyanagi-Harada disease and acute central serous chorioretinopathy. BMC Ophthalmol 2014;14:87.
79. Nakayama M, Keino H, Okada AA, Watanabe T, Taki W, Inoue M, *et al.* Enhanced depth imaging optical coherence tomography of the choroid in Vogt-Koyanagi-Harada disease. Retina 2012;32:2061-9.
80. Pang CE, Messinger JD, Zanzottera EC, Freund KB, Curcio CA. The onion sign in neovascular age-related macular degeneration represents cholesterol crystals. Ophthalmology 2015;122:2316-26.
81. Khan S, Engelbert M, Imamura Y, Freund KB. Polypoidal choroidal vasculopathy: Simultaneous indocyanine green angiography and eye-tracked spectral domain optical coherence tomography findings. Retina 2012;32:1057-68.
82. Querques G, Atmani K, Berboucha E, Martinelli D, Coscas G,

Soubrane G, *et al.* Angiographic analysis of retinal-choroidal anastomosis by confocal scanning laser ophthalmoscopy technology and corresponding (eye-tracked) spectral-domain optical coherence tomography. Retina 2010;30:222-34.

83. Enhanced Depth Imaging Spectral-Domain Optical Coherence Tomography. Available from: http://www.ajo.com/article/S0002-9394(08)00418-2/pdf. [Last accessed on 2017 Aug 15].
84. Adhi M, Liu JJ, Qavi AH, Grulkowski I, Lu CD, Mohler KJ, *et al.* Choroidal analysis in healthy eyes using swept-source optical coherence tomography compared to spectral domain optical coherence tomography. Am J Ophthalmol 2014;157:1272-810.
85. Adhi M, Liu JJ, Qavi AH, Grulkowski I, Fujimoto JG, Duker JS, *et al.* Enhanced visualization of the choroido-scleral interface using swept-source OCT. Ophthalmic Surg Lasers Imaging Retina 2013;44:S40-2.
86. Ferrara D, Waheed NK, Duker JS. Investigating the choriocapillaris and choroidal vasculature with new optical coherence tomography technologies. Prog Retin Eye Res 2016;52:130-55.
87. Mrejen S, Spaide RF. Optical coherence tomography: Imaging of the choroid and beyond. Surv Ophthalmol 2013;58:387-429.
88. Spaide RF. Age-related choroidal atrophy. Am J Ophthalmol 2009;147:801-10.
89. Mahendradas P, Madhu S, Kawali A, Govindaraj I, Gowda PB, Vinekar A, *et al.* Combined depth imaging of choroid in uveitis. J Ophthalmic Inflamm Infect 2014;4:18.
90. Kim JS, Knickelbein JE, Jaworski L, Kaushal P, Vitale S, Nussenblatt RB, *et al.* Enhanced depth imaging optical coherence tomography in uveitis: An intravisit and interobserver reproducibility study. Am J Ophthalmol 2016;164:49-56.
91. Ishibazawa A, Kinouchi R, Minami Y, Katada A, Yoshida A. Recurrent vogt–Koyanagi–Harada disease with sensorineural hearing loss and choroidal thickening. Int Ophthalmol 2014;34:679-84.
92. Dastiridou AI, Bousquet E, Kuehlewein L, Tepelus T, Monnet D, Salah S, *et al.* Choroidal imaging with swept-source optical coherence tomography in patients with birdshot chorioretinopathy: Choroidal reflectivity and thickness. Ophthalmology 2017;124:1186-95.
93. Skvortsova N, Gasc A, Jeannin B, Herbort CP. Evolution of choroidal thickness over time and effect of early and sustained therapy in birdshot retinochoroiditis. Eye (Lond) 2017;31:1205-11.
94. Invernizzi A, Agarwal A, Mapelli C, Nguyen QD, Staurenghi G, Viola F, *et al.* Longitudinal follow-up of choroidal granulomas using enhanced depth imaging optical coherence tomography. Retina 2017;37:144-53.
95. Invernizzi A, Mapelli C, Viola F, Cigada M, Cimino L, Ratiglia R, *et al.* Choroidal granulomas visualized by enhanced depth imaging optical coherence tomography. Retina 2015;35:525-31.
96. Shinohara K, Shimada N, Moriyama M, Yoshida T, Jonas JB, Yoshimura N, *et al.* Posterior staphylomas in pathologic myopia imaged by widefield optical coherence tomography. Invest Ophthalmol Vis Sci 2017;58:3750-8.
97. Shinohara K, Moriyama M, Shimada N, Yoshida T, Ohno-Matsui K. Characteristics of peripapillary staphylomas associated with high myopia determined by swept-source optical coherence tomography. Am J Ophthalmol 2016;169:138-44.
98. García-Ben A, Kamal-Salah R, García-Basterra I, Gonzalez Gómez A, Morillo Sanchez MJ, García-Campos JM, *et al.* Two- and three-dimensional topographic analysis of pathologically myopic eyes with dome-shaped macula and inferior staphyloma by spectral domain optical coherence tomography. Graefes Arch Clin Exp Ophthalmol 2017;255:903-12.
99. Ng DS, Cheung CY, Luk FO, Mohamed S, Brelen ME, Yam JC, *et al.* Advances of optical coherence tomography in myopia and pathologic myopia. Eye (Lond) 2016;30:901-16.
100. Ohsugi H, Ikuno Y, Oshima K, Yamauchi T, Tabuchi H. Morphologic characteristics of macular complications of a dome-shaped macula determined by swept-source optical coherence tomography. Am J Ophthalmol 2014;158:162-700.
101. Ellabban AA, Tsujikawa A, Matsumoto A, Yamashiro K, Oishi A, Ooto S, *et al.* Three-dimensional tomographic features of dome-shaped macula by swept-source optical coherence tomography. Am J Ophthalmol 2013;155:320-800.
102. Lee KM, Woo SJ, Hwang JM. Evaluation of congenital excavated optic disc anomalies with spectral-domain and swept-source optical coherence tomography. Graefes Arch Clin Exp Ophthalmol 2014;252:1853-60.
103. Jeng-Miller KW, Cestari DM, Gaier ED. Congenital anomalies of the optic disc: Insights from optical coherence tomography imaging. Curr Opin Ophthalmol 2017;28:579-86.
104. Ohno-Matsui K, Hirakata A, Inoue M, Akiba M, Ishibashi T. Evaluation of congenital optic disc pits and optic disc colobomas by swept-source optical coherence tomography. Invest Ophthalmol Vis Sci 2013;54:7769-78.
105. Wintergerst MWM, Schultz T, Birtel J, Schuster AK, Pfeiffer N, Schmitz-Valckenberg S, *et al.* Algorithms for the automated analysis of age-related macular degeneration biomarkers on optical coherence tomography: A Systematic review. Transl Vis Sci Technol 2017;6:10.
106. Ehlers JP. Intraoperative optical coherence tomography: Past, present, and future. Eye (Lond) 2016;30:193-201.
107. Hahn P, Migacz J, O'Donnell R, Day S, Lee A, Lin P, *et al.* Preclinical evaluation and intraoperative human retinal imaging with a high-resolution microscope-integrated spectral domain optical coherence tomography device. Retina 2013;33:1328-37.
108. Reznicek L, Klein T, Wieser W, Kernt M, Wolf A, Haritoglou C, *et al.* Megahertz ultra-wide-field swept-source retina optical coherence tomography compared to current existing imaging devices. Graefes Arch Clin Exp Ophthalmol 2014;252:1009-16.
109. Zhang A, Zhang Q, Chen CL, Wang RK. Methods and algorithms for optical coherence tomography-based angiography: A review and comparison. J Biomed Opt 2015;20:100901.
110. Pircher M, Zawadzki RJ. Review of adaptive optics OCT (AO-OCT): Principles and applications for retinal imaging [Invited]. Biomed Opt Express 2017;8:2536-62.